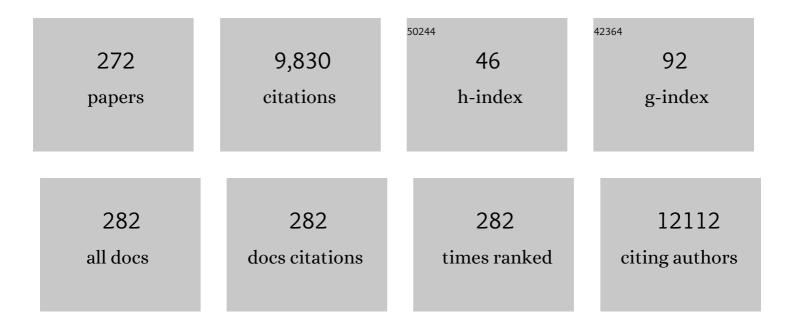
## Mowafak M Al-Jassim

List of Publications by Year in descending order

Source: https://exaly.com/author-pdf/6101685/publications.pdf Version: 2024-02-01



#	Article	IF	CITATIONS
1	Carrier lifetimes of >1 μs in Sn-Pb perovskites enable efficient all-perovskite tandem solar cells. Science, 2019, 364, 475-479.	6.0	781
2	Band Edge Electronic Structure of BiVO <sub>4</sub> : Elucidating the Role of the Bi s and V d Orbitals. Chemistry of Materials, 2009, 21, 547-551.	3.2	624
3	Employing Lead Thiocyanate Additive to Reduce the Hysteresis and Boost the Fill Factor of Planar Perovskite Solar Cells. Advanced Materials, 2016, 28, 5214-5221.	11.1	487
4	Extrinsic ion migration in perovskite solar cells. Energy and Environmental Science, 2017, 10, 1234-1242.	15.6	458
5	The 2020 photovoltaic technologies roadmap. Journal Physics D: Applied Physics, 2020, 53, 493001.	1.3	274
6	Grain-Boundary-Enhanced Carrier Collection in CdTe Solar Cells. Physical Review Letters, 2014, 112, 156103.	2.9	258
7	Reducing Saturationâ€Current Density to Realize Highâ€Efficiency Lowâ€Bandgap Mixed Tin–Lead Halide Perovskite Solar Cells. Advanced Energy Materials, 2019, 9, 1803135.	10.2	255
8	Electrodeposited Aluminum-Doped α-Fe <sub>2</sub> O <sub>3</sub> Photoelectrodes: Experiment and Theory. Chemistry of Materials, 2010, 22, 510-517.	3.2	240
9	Cooperative tin oxide fullerene electron selective layers for high-performance planar perovskite solar cells. Journal of Materials Chemistry A, 2016, 4, 14276-14283 Comparative study of the luminescence and intrinsic point defects in the kesterite Cu <mml:math display="inline" xmlns:mml="http://www.w3.org/1998/Math/MathML"><mml:msub><mml:msub><mml:mrow< td=""><td>5.2</td><td>204</td></mml:mrow<></mml:msub></mml:msub></mml:math>	5.2	204
10	/> <mml:mn>2</mml:mn> ZnSnS <mml:math xmlns:mml="http://www.w3.org/1998/Math/MathML" display="inline"&gt;<mml:msub><mml:mrow /&gt;<mml:mn>4</mml:mn></mml:mrow </mml:msub>and chalcopyrite Cu(In,Ga)Se<mml:math< td=""><td>1.1</td><td>202</td></mml:math<></mml:math 	1.1	202
11	xmlns:mml="http://www.w3.org/1998/Math/MathML" display="inline"> < mml:msub> < mml:mrow /> < mml: Evaluation of Nitrogen Doping of Tungsten Oxide for Photoelectrochemical Water Splitting. Journal of Physical Chemistry C, 2008, 112, 5213-5220.	1.5	191
12	Understanding and Eliminating Hysteresis for Highly Efficient Planar Perovskite Solar Cells. Advanced Energy Materials, 2017, 7, 1700414.	10.2	190
13	Low-bandgap mixed tin–lead iodide perovskites with reduced methylammonium for simultaneous enhancement of solar cell efficiency and stability. Nature Energy, 2020, 5, 768-776.	19.8	165
14	Mechanisms of Electron-Beam-Induced Damage in Perovskite Thin Films Revealed by Cathodoluminescence Spectroscopy. Journal of Physical Chemistry C, 2015, 119, 26904-26911.	1.5	153
15	Achieving a high open-circuit voltage in inverted wide-bandgap perovskite solar cells with a graded perovskite homojunction. Nano Energy, 2019, 61, 141-147.	8.2	152
16	Enhanced photoelectrochemical responses of ZnO films through Ga and N codoping. Applied Physics Letters, 2007, 91, .	1.5	144
17	Electronic, structural, and magnetic effects of 3d transition metals in hematite. Journal of Applied Physics, 2010, 107, .	1.1	135
18	Engineering Grain Boundaries in Cu <sub>2</sub> ZnSnSe <sub>4</sub> for Better Cell Performance: A Firstâ€Principle Study. Advanced Energy Materials, 2014, 4, 1300712.	10.2	135

#	Article	IF	CITATIONS
19	A graded catalytic–protective layer for an efficient and stable water-splitting photocathode. Nature Energy, 2017, 2, .	19.8	135
20	Arylammonium-Assisted Reduction of the Open-Circuit Voltage Deficit in Wide-Bandgap Perovskite Solar Cells: The Role of Suppressed Ion Migration. ACS Energy Letters, 2020, 5, 2560-2568.	8.8	131
21	Combinatorial insights into doping control and transport properties of zinc tin nitride. Journal of Materials Chemistry C, 2015, 3, 11017-11028.	2.7	128
22	Band-Engineered Bismuth Titanate Pyrochlores for Visible Light Photocatalysis. Journal of Physical Chemistry C, 2010, 114, 10598-10605.	1.5	126
23	Enhancement of photoelectrochemical response by aligned nanorods in ZnO thin films. Journal of Power Sources, 2008, 176, 387-392.	4.0	115
24	Synthesis of band-gap-reduced p-type ZnO films by Cu incorporation. Journal of Applied Physics, 2007, 102, .	1.1	114
25	Direct observation of Na and O impurities at grain surfaces of CulnSe2 thin films. Journal of Vacuum Science and Technology A: Vacuum, Surfaces and Films, 1999, 17, 291-296.	0.9	98
26	ZnO nanocoral structures for photoelectrochemical cells. Applied Physics Letters, 2008, 93, 163117.	1.5	92
27	Electrochemical deposition of copper oxide nanowires for photoelectrochemical applications. Journal of Materials Chemistry, 2010, 20, 6962.	6.7	91
28	Overcoming Carrier Concentration Limits in Polycrystalline CdTe Thin Films with In Situ Doping. Scientific Reports, 2018, 8, 14519.	1.6	84
29	Photoelectrochemical Properties of N-Incorporated ZnO Films Deposited by Reactive RF Magnetron Sputtering. Journal of the Electrochemical Society, 2007, 154, B956.	1.3	81
30	From atomic structure to photovoltaic properties in CdTe solar cells. Ultramicroscopy, 2013, 134, 113-125.	0.8	80
31	In situ investigation of the formation and metastability of formamidinium lead tri-iodide perovskite solar cells. Energy and Environmental Science, 2016, 9, 2372-2382.	15.6	79
32	Cathodoluminescence of Cu(In,Ga)Se2 thin films used in high-efficiency solar cells. Applied Physics Letters, 2003, 83, 4770-4772.	1.5	78
33	Mechanism of Zn and Si diffusion from a highly doped tunnel junction for InGaP/GaAs tandem solar cells. Journal of Applied Physics, 1999, 85, 1481-1486.	1.1	77
34	Understanding the Formation and Temperature Dependence of Thick-Film Ag Contacts on High-Sheet-Resistance Si Emitters for Solar Cells. Journal of the Electrochemical Society, 2005, 152, G742.	1.3	69
35	Perovskite Photovoltaics: The Path to a Printable Terawatt-Scale Technology. ACS Energy Letters, 2017, 2, 2540-2544.	8.8	64
36	Ternary cobalt spinel oxides for solar driven hydrogen production: Theory and experiment. Energy and Environmental Science, 2009, 2, 774.	15.6	60

#	Article	IF	CITATIONS
37	An x-ray photoelectron spectroscopy investigation of O impurity chemistry in CdS thin films grown by chemical bath deposition. Journal of Applied Physics, 1997, 81, 1978-1984.	1.1	56
38	Synthesis and characterization of band gap-reduced ZnO:N and ZnO:(Al,N) films for photoelectrochemical water splitting. Journal of Materials Research, 2010, 25, 69-75.	1.2	56
39	Junction Quality of SnO <sub>2</sub> -Based Perovskite Solar Cells Investigated by Nanometer-Scale Electrical Potential Profiling. ACS Applied Materials & Interfaces, 2017, 9, 38373-38380.	4.0	56
40	Three-dimensional electronic resistivity mapping of solid electrolyte interphase on Si anode materials. Nano Energy, 2019, 55, 477-485.	8.2	56
41	Direct evidence of enhanced chlorine segregation at grain boundaries in polycrystalline CdTe thin films via threeâ€dimensional TOFâ€SIMS imaging. Progress in Photovoltaics: Research and Applications, 2015, 23, 838-846.	4.4	53
42	Physics of grain boundaries in polycrystalline photovoltaic semiconductors. Journal of Applied Physics, 2015, 117, .	1.1	52
43	Defect segregation at grain boundary and its impact on photovoltaic performance of CuInSe2. Applied Physics Letters, 2013, 102, .	1.5	50
44	Obtaining Large Columnar CdTe Grains and Long Lifetime on Nanocrystalline CdSe, MgZnO, or CdS Layers. Advanced Energy Materials, 2018, 8, 1702666.	10.2	49
45	Sodium Accumulation at Potential-Induced Degradation Shunted Areas in Polycrystalline Silicon Modules. IEEE Journal of Photovoltaics, 2016, 6, 1440-1445.	1.5	48
46	Influence of gas ambient on the synthesis of co-doped ZnO:(Al,N) films for photoelectrochemical water splitting. Journal of Power Sources, 2010, 195, 5801-5805.	4.0	47
47	Toward All-Solid-State Lithium Batteries: Three-Dimensional Visualization of Lithium Migration in β-Li <sub>3</sub> PS <sub>4</sub> Ceramic Electrolyte. Journal of the Electrochemical Society, 2018, 165, A3732-A3737.	1.3	46
48	Temperature-Dependent Solubility of Solid Electrolyte Interphase on Silicon Electrodes. ACS Energy Letters, 2019, 4, 2770-2775.	8.8	45
49	Hydrothermally synthesized titania nanotubes as a promising electron transport medium in dye sensitized solar cells exhibiting a record efficiency of 7.6% for 1-D based devices. Journal of Materials Chemistry A, 2013, 1, 5377.	5.2	43
50	Built-in Potential and Charge Distribution within Single Heterostructured Nanorods Measured by Scanning Kelvin Probe Microscopy. Nano Letters, 2013, 13, 1278-1284.	4.5	43
51	Cathodoluminescence of Cu diffusion in CdTe thin films for CdTe/CdS solar cells. Applied Physics Letters, 2002, 81, 2962-2964.	1.5	42
52	Prediction of the chemical trends of oxygen vacancy levels in binary metal oxides. Applied Physics Letters, 2011, 99, .	1.5	42
53	Understanding the charge transport mechanisms through ultrathin SiO <i>x</i> layers in passivated contacts for high-efficiency silicon solar cells. Applied Physics Letters, 2019, 114, .	1.5	41
54	Grain engineering: How nanoscale inhomogeneities can control charge collection in solar cells. Nano Energy, 2017, 32, 488-493.	8.2	40

4

#	Article	IF	CITATIONS
55	Templated Growth and Passivation of Vertically Oriented Antimony Selenide Thin Films for Highâ€Efficiency Solar Cells in Substrate Configuration. Advanced Functional Materials, 2022, 32, 2110032.	7.8	40
56	On the existence of Si–C double bonded graphene-like layers. Chemical Physics Letters, 2009, 479, 255-258.	1.2	39
57	Inhomogeneous Doping of Perovskite Materials by Dopants from Hole-Transport Layer. Matter, 2020, 2, 261-272.	5.0	38
58	Structural, electronic, and optical properties of Cu3-V-VI4 compound semiconductors. Applied Physics Letters, 2013, 103, .	1.5	36
59	Imaging of Resonant Quenching of Surface Plasmons by Quantum Dots. Nano Letters, 2006, 6, 2833-2837.	4.5	33
60	Atomic structure of In2O3–ZnO systems. Applied Physics Letters, 2007, 90, 261904.	1.5	32
61	CoAl2O4–Fe2O3 p-n nanocomposite electrodes for photoelectrochemical cells. Applied Physics Letters, 2009, 95, 022116.	1.5	32
62	Beam injection methods for characterizing thin-film solar cells. Progress in Photovoltaics: Research and Applications, 2002, 10, 445-455.	4.4	31
63	Improved current collection in WO <sub>3</sub> :Mo/WO <sub>3</sub> bilayer photoelectrodes. Journal of Materials Research, 2010, 25, 45-51.	1.2	31
64	Nanoscale insight into the pâ€n junction of alkaliâ€incorporated Cu(In,Ga)Se 2 solar cells. Progress in Photovoltaics: Research and Applications, 2017, 25, 764-772.	4.4	31
65	Perovskite quantum dot solar cells: Mapping interfacial energetics for improving charge separation. Nano Energy, 2020, 78, 105319.	8.2	31
66	Understanding and Use of IR Belt Furnace for Rapid Thermal Firing of Screen-Printed Contacts to Si Solar Cells. IEEE Electron Device Letters, 2010, 31, 461-463.	2.2	30
67	Enhancing the Stability of CuO Thin-Film Photoelectrodes by Ti Alloying. Journal of Electronic Materials, 2012, 41, 3062-3067.	1.0	30
68	Titanium and magnesium Co-alloyed hematite thin films for photoelectrochemical water splitting. Journal of Applied Physics, 2012, 111, 073502.	1.1	30
69	Effect of Crystallographic Orientation and Nanoscale Surface Morphology on Poly-Si/SiO <sub><i>x</i></sub> Contacts for Silicon Solar Cells. ACS Applied Materials & Interfaces, 2019, 11, 42021-42031.	4.0	29
70	Synthesis and characterization of titanium-alloyed hematite thin films for photoelectrochemical water splitting. Journal of Applied Physics, 2011, 110, .	1.1	28
71	Origin of the diverse behavior of oxygen vacancies inABO3perovskites: A symmetry based analysis. Physical Review B, 2012, 85, .	1.1	28
72	Identification and analysis of partial shading breakdown sites in CuInxGa(1-x)Se2 modules. Solar Energy, 2018, 161, 1-5.	2.9	28

#	Article	IF	CITATIONS
73	Mott insulators: An early selection criterion for materials for photoelectrochemical H2 production. Journal of Renewable and Sustainable Energy, 2011, 3, .	0.8	27
74	Possible effects of oxygen in Te-rich Σ3 (112) grain boundaries in CdTe. Solid State Communications, 2012, 152, 1744-1747.	0.9	27
75	Quantitative Determination of Grain-Boundary Recombination Velocity in CdTe by Cathodoluminescence Measurements and Numerical Simulations. IEEE Journal of Photovoltaics, 2015, 5, 1722-1726.	1.5	27
76	Effect of Water Vapor, Temperature, and Rapid Annealing on Formamidinium Lead Triiodide Perovskite Crystallization. ACS Energy Letters, 2016, 1, 155-161.	8.8	27
77	Nanocrystal formation in annealed a-SiO0.17N0.07:H films. Nanotechnology, 2004, 15, 1831-1836.	1.3	26
78	Low-temperature silicon homoepitaxy by hot-wire chemical vapor deposition with a Ta filament. Journal of Crystal Growth, 2006, 287, 414-418.	0.7	26
79	Phase separation in Ga and N co-incorporated ZnO films and its effects on photo-response in photoelectrochemical water splitting. Thin Solid Films, 2011, 519, 5983-5987.	0.8	26
80	Investigating PID shunting in polycrystalline silicon modules via multiscale, multitechnique characterization. Progress in Photovoltaics: Research and Applications, 2018, 26, 377-384.	4.4	26
81	Microscopic Observation of Solid Electrolyte Interphase Bilayer Inversion on Silicon Oxide. ACS Energy Letters, 2020, 5, 3657-3662.	8.8	26
82	Photon emission in CuInSe2 thin films observed by scanning tunneling microscopy. Applied Physics Letters, 2005, 86, 143115.	1.5	25
83	Cathodoluminescence Analysis of Grain Boundaries and Grain Interiors in Thin-Film CdTe. IEEE Journal of Photovoltaics, 2014, 4, 1671-1679.	1.5	25
84	LDA+U/GGA+U calculations of structural and electronic properties of CdTe: Dependence on the effective U parameter. Computational Materials Science, 2015, 98, 18-23.	1.4	25
85	Luminescence methodology to determine grain-boundary, grain-interior, and surface recombination in thin-film solar cells. Journal of Applied Physics, 2018, 124, .	1.1	25
86	Impact of dopant-induced optoelectronic tails on open-circuit voltage in arsenic-doped Cd(Se)Te solar cells. Journal of Applied Physics, 2020, 128, .	1.1	25
87	Lateral electron transport in Cu(In,Ga)Se2 investigated by electro-assisted scanning tunneling microscopy. Applied Physics Letters, 2005, 87, 172106.	1.5	24
88	Revealing Surface Modifications of Potassiumâ€Fluorideâ€Treated Cu(In,Ga)Se <sub>2</sub> : A Study of Material Structure, Chemistry, and Photovoltaic Performance. Advanced Materials Interfaces, 2016, 3, 1600013	1.9	24
89	In < mml:math xmlns:mml="http://www.w3.org/1998/Math/MathML" display="inline"> < mml:msub> < mml:mrow /> < mml:mn> 2 < /mml:mn> < /mml:msub> < /mml:math> O < mml:math xmlns:mml="http://www.w3.org/1998/Math/MathML" display="inline"> < mml:msub> < mml:mrow	1.1	23
90	<ul> <li>Amins. Inite - Fitte, //www.ws.olg/1998/Wath/Wath/We display= Inite &gt; (Inite &gt; (</li></ul>	7.3	23

#	Article	IF	CITATIONS
91	Comprehensive characterization of CICS absorber layers grown by one-step sputtering process. Ceramics International, 2019, 45, 4424-4430.	2.3	22
92	Nonuniform Ionic and Electronic Transport of Ceramic and Polymer/Ceramic Hybrid Electrolyte by Nanometerâ€Scale Operando Imaging for Solidâ€State Battery. Advanced Energy Materials, 2020, 10, 2000219.	10.2	22
93	Bandgap engineering of Cu(In_1-xGa_x)Se_2 absorber layers fabricated using CuInSe_2 and CuGaSe_2 targets for one-step sputtering process. Optical Materials Express, 2016, 6, 3541.	1.6	21
94	Impact of Wide-Ranging Nanoscale Chemistry on Band Structure at Cu(In, Ga)Se2 Grain Boundaries. Scientific Reports, 2017, 7, 14163.	1.6	21
95	Carrier diffusion and radiative recombination in CdTe thin films. Applied Physics Letters, 2002, 81, 3161-3163.	1.5	20
96	Symmetry-breaking-induced enhancement of visible light absorption in delafossite alloys. Applied Physics Letters, 2009, 94, 251907.	1.5	20
97	Evolution of solid electrolyte interphase and active material in the silicon wafer model system. Journal of Power Sources, 2021, 482, 228946.	4.0	19
98	Transmission electron microscopy of chalcogenide thin-film photovoltaic materials. Current Opinion in Solid State and Materials Science, 2012, 16, 39-44.	5.6	18
99	Influence of CdTe Deposition Temperature and Window Thickness on CdTe Grain Size and Lifetime After CdCl 2 Recrystallization. IEEE Journal of Photovoltaics, 2018, 8, 600-603.	1.5	18
100	Sub-Bandgap Luminescence from Doped Polycrystalline and Amorphous Silicon Films and Its Application to Understanding Passivating-Contact Solar Cells. ACS Applied Energy Materials, 2018, 1, 6619-6625.	2.5	18
101	Protection of GaInP <sub>2</sub> Photocathodes by Direct Photoelectrodeposition of MoS <i><sub>x</sub></i> Thin Films. ACS Applied Materials & Interfaces, 2019, 11, 25115-25122.	4.0	18
102	No Evidence for Passivation Effects of Na and K at Grain Boundaries in Polycrystalline Cu(In,Ga)Se <sub>2</sub> Thin Films for Solar Cells. Solar Rrl, 2019, 3, 1900095.	3.1	18
103	Imaging Spatial Variations of Optical Bandgaps in Perovskite Solar Cells. Advanced Energy Materials, 2019, 9, 1802790.	10.2	18
104	Effect of Surface Texture on Pinhole Formation in SiO <i><sub>x</sub></i> -Based Passivated Contacts for High-Performance Silicon Solar Cells. ACS Applied Materials & Interfaces, 2020, 12, 55737-55745.	4.0	18
105	Failure analysis of fieldâ€failed bypass diodes. Progress in Photovoltaics: Research and Applications, 2020, 28, 909-918.	4.4	18
106	Effect of substrate temperature on the photoelectrochemical responses of Ga and N co-doped ZnO films. Journal of Materials Science, 2010, 45, 5218-5222.	1.7	17
107	Origin of Bonding between the SWCNT and the Fe <sub>3</sub> O <sub>4</sub> (001) Surface and the Enhanced Electrical Conductivity. Journal of Physical Chemistry Letters, 2011, 2, 2853-2858.	2.1	17
108	The effects of Bi alloying in Cu delafossites: A density functional theory study. Journal of Applied Physics, 2011, 109, .	1.1	17

#	Article	IF	CITATIONS
109	Measurement of semiconductor surface potential using the scanning electron microscope. Journal of Applied Physics, 2012, 111, .	1.1	17
110	3-D point defect density distributions in thin film Cu(In,Ga)Se2 measured by atom probe tomography. Acta Materialia, 2016, 102, 32-37.	3.8	17
111	Fabrication and Characterization of CZTS Thin Films Prepared by the Sulfurization of RF-Sputtered Stacked Metal Precursors. Journal of Electronic Materials, 2014, 43, 3145-3154.	1.0	16
112	Destructive reverse bias pinning in perovskite/silicon tandem solar modules caused by perovskite hysteresis under dynamic shading. Sustainable Energy and Fuels, 2020, 4, 4067-4075.	2.5	16
113	Morphology, microstructure, and doping behaviour: A comparison between different deposition methods for polyâ€6i/SiO <sub><i>x</i>&gt; passivating contacts. Progress in Photovoltaics: Research and Applications, 2021, 29, 857-868.</sub>	4.4	16
114	Electronic and optical properties of Co <i>X</i> 2O4 ( <i>X</i> = Al, Ga, In) alloys. Applied Physics Letters, 2012, 100, .	1.5	15
115	Latest developments in the x-ray based characterization of thin-film solar cells. , 2015, , .		15
116	Amorphous copper tungsten oxide with tunable band gaps. Journal of Applied Physics, 2010, 108, 043502.	1.1	14
117	SMART Perovskite Growth: Enabling a Larger Range of Process Conditions. ACS Energy Letters, 2021, 6, 650-658.	8.8	14
118	New Polytypoid SnO <sub>2</sub> (ZnO:Sn) <sub><i>m</i></sub> Nanowire: Characterization and Calculation of Its Electronic Structure. Journal of Physical Chemistry C, 2012, 116, 5009-5013.	1.5	13
119	Defectâ€band photoluminescence imaging on multiâ€crystalline silicon wafers. Physica Status Solidi - Rapid Research Letters, 2012, 6, 190-192.	1.2	13
120	Effect of gas ambient and varying RF sputtering power for bandgap narrowing of mixed (ZnO:GaN) thin films for solar driven hydrogen production. Journal of Power Sources, 2013, 232, 74-78.	4.0	13
121	Contrasting the Material Chemistry of Cu <sub>2</sub> ZnSnSe <sub>4</sub> and Cu <sub>2</sub> ZnSnS <sub>(4–</sub> <i><sub>x</sub></i> <sub>)</sub> Se <i><sub>x</sub></i> . Advanced Science, 2016, 3, 1500320.	5.6	13
122	Modifications of Textured Silicon Surface Morphology and Its Effect on Poly-Si/SiO <i> <sub>x</sub> </i> Contact Passivation for Silicon Solar Cells. IEEE Journal of Photovoltaics, 2019, 9, 1513-1521.	1.5	13
123	Hydrogenation Mechanisms of Poly‣i/SiO <sub><i>x</i></sub> Passivating Contacts by Different Capping Layers. Solar Rrl, 2020, 4, 1900476.	3.1	13
124	Spatially Resolved Recombination Analysis of CuIn <sub>x</sub> Ga <sub>1-x</sub> Se <sub>2</sub> Absorbers With Alkali Postdeposition Treatments. IEEE Journal of Photovoltaics, 2018, 8, 1833-1840.	1.5	12
125	Investigating PID Shunting in Polycrystalline CIGS Devices via Multi-Scale, Multi-Technique Characterization. IEEE Journal of Photovoltaics, 2019, 9, 559-564.	1.5	12
126	Hydrogen-Assisted Defect Engineering of Doped Poly-Si Films for Passivating Contact Solar Cells. ACS Applied Energy Materials, 2019, 2, 8783-8791.	2.5	12

#	Article	IF	CITATIONS
127	Nanoscale Imaging of Exciton Transport in Organic Photovoltaic Semiconductors by Tip-Enhanced Tunneling Luminescence. Nano Letters, 2009, 9, 3904-3908.	4.5	11
128	Transmission electron microscopy study of dislocations and interfaces in CdTe solar cells. Thin Solid Films, 2011, 519, 7168-7172.	0.8	11
129	Unusual nonlinear strain dependence of valence-band splitting in ZnO. Physical Review B, 2012, 86, .	1.1	11
130	Cation ratio fluctuations in Cu <sub>2</sub> ZnSnS <sub>4</sub> at the 20 nm length scale investigated by analytical electron microscopy. Physica Status Solidi (A) Applications and Materials Science, 2016, 213, 2392-2399.	0.8	11
131	Strong Attraction and Adhesion Forces of Dust Particles by System Voltages of Photovoltaic Modules. IEEE Journal of Photovoltaics, 2019, 9, 1121-1127.	1.5	11
132	Optical and Structural Properties of High-Efficiency Epitaxial Cu(In,Ga)Se <sub>2</sub> Grown on GaAs. ACS Applied Materials & Interfaces, 2020, 12, 3150-3160.	4.0	11
133	Operando X-ray Tomography Imaging of Solid-State Electrolyte Response to Li Evolution under Realistic Operating Conditions. ACS Applied Energy Materials, 2021, 4, 1346-1355.	2.5	11
134	The Effects of an Oxide Layer on the Kinetics of Metal-Induced Crystallization of a-Si:H. Journal of the Electrochemical Society, 2005, 152, G354.	1.3	10
135	The structure and properties of (aluminum, oxygen) defect complexes in silicon. Journal of Applied Physics, 2013, 114, 063520.	1.1	10
136	Interface Characterization of Single-Crystal CdTe Solar Cells With VOC > 950 mV. IEEE Journal of Photovoltaics, 2016, 6, 1650-1653.	1.5	10
137	Locating the electrical junctions in Cu(In,Ga)Se <sub>2</sub> and Cu <sub>2</sub> ZnSnSe <sub>4</sub> solar cells by scanning capacitance spectroscopy. Progress in Photovoltaics: Research and Applications, 2017, 25, 33-40.	4.4	10
138	Hydrogenation Mechanisms of Poly‧i/SiO <sub><i>x</i></sub> Passivating Contacts by Different Capping Layers. Solar Rrl, 2020, 4, 2070033.	3.1	10
139	Advantages of using piezoelectric quantum structures for photovoltaics. Journal of Applied Physics, 2003, 93, 626-631.	1.1	9
140	Correlation between grain composition and charge carrier collection in Cu(In,Ga)Se2 solar cells. , 2015, , .		9
141	Microscopic Real-Space Resistance Mapping Across CdTe Solar Cell Junctions by Scanning Spreading Resistance Microscopy. IEEE Journal of Photovoltaics, 2015, 5, 395-400.	1.5	9
142	Suppression of the <inline-formula><tex-math>\${hbox{Cu}}_{2-x}{hbox{S}}\$</tex-math></inline-formula> Secondary Phases in CZTS Films Through Controlling the Film Elemental Composition. IEEE Journal of Photovoltaics, 2015, 5, 1470-1475.	1.5	9
143	Cathodoluminescence spectrum imaging analysis of CdTe thin-film bevels. Journal of Applied Physics, 2016, 120, .	1.1	9
144	Near-field transport imaging applied to photovoltaic materials. Solar Energy, 2017, 153, 134-141.	2.9	9

#	Article	IF	CITATIONS
145	Thin-Film Module Reverse-Bias Breakdown Sites Identified by Thermal Imaging. , 2018, , .		9
146	Effect of Window-Layer Materials on p-n Junction Location in Cu(In,Ga)Se <sub>2</sub> Solar Cells. IEEE Journal of Photovoltaics, 2019, 9, 308-312.	1.5	9
147	TfC17. Microstructural, compositional and electrical characterization of ferroelectric lead zirconate titanate thin films. Ferroelectrics, 1992, 134, 303-312.	0.3	8
148	Effects of hydrogen on the growth of nanocrystalline silicon films by electron-beam excited plasma chemical vapor deposition. Journal of Applied Physics, 2000, 88, 6848-6855.	1.1	8
149	Cu(In,Ga)Se <sub>2</sub> Thin-Film Evolution During Growth from (In,Ga) <sub>2</sub> Se <sub>3</sub> Precursors. Materials Research Society Symposia Proceedings, 2001, 668, 1.	0.1	8
150	Comparison of photoluminescence imaging on starting multi-crystalline silicon wafers to finished cell performance. , 2012, , .		8
151	Direct imaging of enhanced current collection on grain boundaries of Cu(In,Ga)Se2 solar cells. Applied Physics Letters, 2014, 104, .	1.5	8
152	Characterization and modeling of reverseâ€bias breakdown in Cu(In,Ga)Se <sub>2</sub> photovoltaic devices. Progress in Photovoltaics: Research and Applications, 2019, 27, 812-823.	4.4	8
153	10% efficiency Cu(In,Ga)Se2 solar cell with strongly (220)/(204) oriented Cu-poor absorber layers sputtered using single quaternary target. Journal of Alloys and Compounds, 2020, 812, 152065.	2.8	8
154	Trap-Assisted Dopant Compensation Prevents Shunting in Poly-Si Passivating Interdigitated Back Contact Silicon Solar Cells. ACS Applied Energy Materials, 2021, 4, 10774-10782.	2.5	8
155	TEM study of Locations of Cu in CdTe Solar Cells. Materials Research Society Symposia Proceedings, 2007, 1012, 1.	0.1	7
156	Effect of grain alignment on lateral carrier transport in aligned-crystalline silicon films on polycrystalline substrates. Journal of Materials Research, 2007, 22, 821-825.	1.2	7
157	SiO <inf>2</inf> as barrier layer for Na out-diffusion from soda-lime glass. , 2010, , .		7
158	Synthesis and Characterization of Magnesium-Alloyed Hematite Thin Films. Journal of Electronic Materials, 2012, 41, 3100-3106.	1.0	7
159	Creating intermediate bands in ZnTe via co-alloying approach. Applied Physics Express, 2014, 7, 121201.	1.1	7
160	Module degradation mechanisms studied by a multi-scale approach. , 2016, , .		7
161	In situ investigation of halide incorporation into perovskite solar cells. MRS Communications, 2017, 7, 575-582.	0.8	7
162	Development of in-situ high-voltage and high-temperature stressing capability on atomic force microscopy platform. Solar Energy, 2017, 158, 746-752.	2.9	7

Mowafak M Al-Jassim

#	Article	IF	CITATIONS
163	Tunneling or Pinholes: Understanding the Transport Mechanisms in SiO <inf>x</inf> Based Passivated Contacts for High-Efficiency Silicon Solar Cells. , 2018, , .		7
164	Defect Detection in Solid-State Battery Electrolytes Using Lock-In Thermal Imaging. Journal of the Electrochemical Society, 2018, 165, A3205-A3211.	1.3	7
165	Largeâ€Area Material and Junction Damage in c–Si Solar Cells by Potentialâ€Induced Degradation. Solar Rrl, 2019, 3, 1800303.	3.1	7
166	Three-Dimensional Mapping of Resistivity and Microstructure of Composite Electrodes for Lithium-Ion Batteries. Nano Letters, 2020, 20, 8081-8088.	4.5	7
167	Application of electron backscatter diffraction techniques to quantify effects of aging on sub-grain and spatial heterogeneity in NMC cathodes. Energy Storage Materials, 2022, 44, 342-352.	9.5	7
168	Advances in Coring Procedures of Silicon Photovoltaic Modules. , 2020, , .		7
169	Electron-Backscatter Diffraction of Photovoltaic Thin Films. Materials Research Society Symposia Proceedings, 2007, 1012, 1.	0.1	6
170	Effects of substrate temperature and RF power on the formation of aligned nanorods in ZnO thin films. Jom, 2010, 62, 25-30.	0.9	6
171	Origin of charge separation in III-nitride nanowires under strain. Applied Physics Letters, 2011, 99, 262103.	1.5	6
172	ZnO:GaN thin films for photoelectrochemical water splitting application. Emerging Materials Research, 2012, 1, 201-204.	0.4	6
173	Strong asymmetrical doping properties of spinel CoAl2O4. Journal of Applied Physics, 2012, 111, 093723.	1.1	6
174	Phosphorus doping of polycrystalline CdTe by diffusion. , 2015, , .		6
175	Quantification of Sheet Resistance in Boronâ€Diffused Silicon Using Microâ€Photoluminescence Spectroscopy at Room Temperature. Solar Rrl, 2017, 1, 1700088.	3.1	6
176	NREL Efforts to Address Soiling on PV Modules. , 2017, , .		6
177	TEM Investigation of the Role of a Nano-oxide Layer in Aluminum-Induced Crystallization of a-Si:H. Electrochemical and Solid-State Letters, 2006, 9, G225.	2.2	5
178	Quality characterization of silicon bricks using photoluminescence imaging and photoconductive decay. , 2012, , .		5
179	A comparative study of the defect point physics and luminescence of the kesterites Cu <inf>2</inf> ZnSnS <inf>4</inf> and Cu <inf>2</inf> ZnSnSe <inf>4</inf> and chalcopyrite Cu(In.Ga)Se<:inf>2<:/inf>:, , 2012		5
180	Alkali segregation and matrix concentrations in thin film Cu(In,Ga)Se2 at targeted interfaces characterized in 3-D at the nanoscale. , 2015, , .		5

#	Article	IF	CITATIONS
181	Semi-statistical Atom Probe Tomography Analysis of Thin Film Grain Boundaries. Microscopy and Microanalysis, 2016, 22, 644-645.	0.2	5
182	Spatial luminescence imaging of dopant incorporation in CdTe Films. Journal of Applied Physics, 2017, 121, 045304.	1.1	5
183	Identifying Reverse-Bias Breakdown Sites in CulnxGa(1-x)Se2. , 2017, , .		5
184	High-Throughput Experimental Study of Wurtzite Mn1–xZnxO Alloys for Water Splitting Applications. ACS Omega, 2019, 4, 7436-7447.	1.6	5
185	Perovskite Solar Cells: Imaging Spatial Variations of Optical Bandgaps in Perovskite Solar Cells (Adv.) Tj ETQq1 1	0.784314 10.2	l rgBT /Over <mark>l</mark> o
186	Solid State Electrolytes: Nonuniform Ionic and Electronic Transport of Ceramic and Polymer/Ceramic Hybrid Electrolyte by Nanometerâ€scale Operando Imaging for Solidâ€state Battery (Adv. Energy Mater.) Tj ETQ	q01 <b>0.0</b> rgł	BT Øverlock I
187	Imaging <mml:math xmlns:mml="http://www.w3.org/1998/Math/MathML"><mml:msub><mml:mi mathvariant="normal"&gt;CdCl<mml:mn>2</mml:mn></mml:mi </mml:msub></mml:math> defect passivation and formation in polycrystalline CdTe films by cathodoluminescence. Physical Review Materials. 2021. 5	0.9	5
188	Optimization of vertical and lateral distances between target and substrate in deposition process of CuGaSe <sub>2</sub> thin films using one-step sputtering. Materials Express, 2017, 7, 35-42.	0.2	5
189	Plasmon excitations in scanning tunneling microscopy: Simultaneous imaging of modes with different localizations coupled at the tip. Applied Physics Letters, 2007, 90, 193109.	1.5	4
190	Imaging study of multi-crystalline silicon wafers throughout the manufacturing process. , 2011, , .		4
191	The delocalized nature of holes in (Ga, N) cluster-doped ZnO. Journal of Physics Condensed Matter, 2012, 24, 415503.	0.7	4
192	Photoelectrochemical behavior of mixed ZnO and GaN (ZnO:GaN) thin films prepared by sputtering technique. Applied Surface Science, 2013, 270, 718-721.	3.1	4
193	Defect characterization in compositionally graded InGaAs layers on GaAs(001) grown by MBE. Physica Status Solidi C: Current Topics in Solid State Physics, 2013, 10, 1640-1643.	0.8	4
194	Synchrotron x-ray characterization of alkali elements at grain boundaries in Cu(In, Ga)Se <inf>2</inf> solar cells. , 2016, , .		4
195	Three-dimensional minority-carrier collection channels at shunt locations in silicon solar cells. Solar Energy, 2016, 135, 163-168.	2.9	4
196	Carrier-Transport Study of Gallium Arsenide Hillock Defects. Microscopy and Microanalysis, 2019, 25, 1160-1166.	0.2	4
197	Light- and Elevated-Temperature-Induced Degradation-Affected Silicon Cells From a Utility-Scale Photovoltaic System Characterized by Deep-Level Transient Spectroscopy. IEEE Journal of Photovoltaics, 2022, 12, 703-710.	1.5	4
198	Damage-Layer-Mediated H Diffusion During SiN:H Processing: A Comprehensive Model. , 2006, , .		3

#	Article	IF	CITATIONS
199	Ultrahighâ€Crystallineâ€Quality Silicon Pillars Formed by Millimeterâ€Wave Annealing of Amorphous Silicon on Glass. Advanced Materials, 2009, 21, 3002-3006.	11.1	3
200	Microstructure and surface chemistry of nanoporous "black silicon" for photovoltaics. , 2010, , .		3
201	Atomic scale characterization of compound semiconductors using atom probe tomography. , 2011, , .		3
202	Defect-bandemission photoluminescence imagingonmulti-crystallinesisolar cells. , 2011, , .		3
203	Core Structures of Dislocations within CdTe Grains. Materials Research Society Symposia Proceedings, 2013, 1526, 1.	0.1	3
204	Atomic scale understanding of poly-Si/SiO <inf>2</inf> /c-Si passivated contacts: Passivation degradation due to metallization. , 2016, , .		3
205	Nanometer-scale electrical potential profiling across perovskite solar cells. , 2016, , .		3
206	Imaging the Thickness of Passivation Layers for Crystalline Silicon with Micron cale Spatial Resolution Using Spectral Photoluminescence. Solar Rrl, 2017, 1, 1700157.	3.1	3
207	Investigating PID Shunting in Polycrystalline Silicon Modules via Multi-Scale, Multi-Technique Characterization. , 2017, , .		3
208	Direct Microscopy Imaging of Nonuniform Carrier Transport in Polycrystalline Cadmium Telluride. Cell Reports Physical Science, 2020, 1, 100230.	2.8	3
209	Investigation of Gallium–Boron Spinâ€On Codoping for polyâ€&i/SiO <sub><i>x</i></sub> Passivating Contacts. Solar Rrl, 2021, 5, 2100653.	3.1	3
210	Imaging the solar cell P-N junction and depletion region using secondary electron contrast. , 2011, , .		2
211	Temperature-dependent Photoluminescence imaging and characterization of a multi-crystalline silicon solar cell defect area. , 2011, , .		2
212	Quantification of atomic scale defects in poly Si PV devices using atom probe tomography. , 2012, , .		2
213	Targeting Grain Boundaries for Structural and Chemical Analysis Using Correlative EBSD, TEM and APT. Microscopy and Microanalysis, 2015, 21, 43-44.	0.2	2
214	Predicting a quaternary tungsten oxide for sustainable photovoltaic application by density functional theory. Applied Physics Letters, 2015, 107, 233902.	1.5	2
215	Quantitative determination of grain boundary recombination velocity in CdTe by combination of cathodoluminescence measurements and numerical simulations. , 2015, , .		2

216 Development of scanning capacitance spectroscopy of CIGS solar cells. , 2015, , .

2

#	Article	IF	CITATIONS
217	Evolution of Copper Electrodes Fabricated by Electroless Plating on BaZr0.7Ce0.2Y0.1O3-δ Proton-Conducting Ceramic Membrane: From Deposition to Testing in Methane. Ceramics, 2018, 1, 261-273.	1.0	2
218	Wurtzite materials in alloys of rock salt compounds. Journal of Materials Research, 2020, 35, 972-980.	1.2	2
219	LeTID-affected Cells from a Utility-scale Photovoltaic System Characterized by Deep Level Transient Spectroscopy. , 2021, , .		2
220	Linking Transient Voltage to Spatially-Resolved Luminescence Imaging to Understand Reliability of Perovskite Photovoltaics. , 2021, , .		2
221	Local Resistance Measurement for Degradation of c-Si Heterojunction with Intrinsic Thin Layer (HIT) Solar Modules. , 2020, , .		2
222	Nondestructive microstructural investigation of defects in 4H-SiC epilayers using a multiscale luminescence analysis approach. Journal of Applied Physics, 2022, 131, 185705.	1.1	2
223	Compositional analysis of CdS/SnO2 films after heat treatments and CdCl2 pretreatments. Surface and Interface Analysis, 1994, 21, 160-162.	0.8	1
224	Epitaxial silicon thin films by low-temperature aluminum induced crystallization of amorphous silicon for solar cell applications. , 2006, , .		1
225	Investigation of Charge Trapping at Grain Boundaries in Polycrystalline and Multicrystalline Silicon Solar Cells. Materials Research Society Symposia Proceedings, 2010, 1268, 11.	0.1	1
226	Superior low-light-level performance of upgraded metallurgical-grade silicon modules. , 2012, , .		1
227	Influence of Gas Flow Rate for Formation of Aligned Nanorods in ZnO Thin Films for Solar-Driven Hydrogen Production. Jom, 2012, 64, 526-530.	0.9	1
228	Structural, chemical and luminescent investigation of MBE- and CSS-deposited CdTe thin-films for solar cells. , 2013, , .		1
229	The Effect of Ga Content on the Recombination Behavior of Grain Boundaries in Cu(In,Ga)Se2 Solar Cells. Materials Research Society Symposia Proceedings, 2014, 1670, 19.	0.1	1
230	Direct evidence of a Cu(In,Ga) <inf>3</inf> Se <inf>5</inf> phase in a bulk, high-efficiency Cu(In,Ga)Se <inf>2</inf> device using atom probe tomography. , 2014, , .		1
231	Texture Manipulation and Its Impact on Electrical Properties of Zinc Phosphide Thin Films. Journal of Electronic Materials, 2015, 44, 2566-2573.	1.0	1
232	Opto-electronic characterization of CdTe solar cells from TCO to back contact with nano-scale CL probe. , 2015, , .		1
233	Spectrum-per-pixel cathodoluminescence imaging of CdTe thin-film bevels. , 2016, , .		1
234	Using Time-of-Flight SIMS to Investigate Group V Dopant Distribution in CdTe. , 2017, , .		1

Mowafak M Al-Jassim

#	Article	IF	CITATIONS
235	Analytical (S)TEM Studies of Defects Associated with PID in Stressed Si PV Modules. , 2017, , .		1
236	Photoluminescence-imaging-based Evaluation of Non-uniform CdTe Degradation. , 2017, , .		1
237	Microstructure Study on Initial Lithiation/Delithiation Cycle of Crystalline Silicon Wafer. Microscopy and Microanalysis, 2019, 25, 2098-2099.	0.2	1
238	Comparison of PID Shunting in Polycrystalline and Single-Crystal Silicon Modules via Multi-Scale, Multi-Technique Characterization. , 2019, , .		1
239	Nonuniform Charge Collection in SiO <sub>x</sub> -Based Passivated-Contact Silicon Solar Cells. , 2019, , .		1
240	Epitaxial Silicon Thin Films by Low Temperature Aluminum Induced Crystallization of Amorphous Silicon. Materials Research Society Symposia Proceedings, 2006, 910, 4.	0.1	0
241	Structural, electronic, and optical properties of the In <inf>2</inf> O <inf>3</inf> (ZnO) <inf>n</inf> system. , 2009, , .		Ο
242	Identification and characterization of performance limiting regions in poly-Si wafers for PV cells. , 2011, , .		0
243	A model for electron-beam-induced current analysis of mc-Si addressing defect contrast behavior in heavily contaminated PV material. , 2012, , .		Ο
244	Silicon grain boundary passivation for photovoltaics: A novel approach with small polar molecules. , 2012, , .		0
245	Defect band luminescence intensity reversal as related to application of anti-reflection coating on mc-Si PV Cells. , 2012, , .		Ο
246	Structural and Electro-Optical Properties of CdTe Films Used in CdTe/CdS Solar Cells Grown with Substrate Configuration. Materials Research Society Symposia Proceedings, 2013, 1493, 183-188.	0.1	0
247	Atomic-scale origin of emission from extended defects in mc-Si. , 2013, , .		Ο
248	Electron microscopy study of individual grain boundaries in Cu <inf>2</inf> ZnSnSe <inf>4</inf> thin films. , 2013, , .		0
249	First principles study of aluminum-oxygen complexes in silicon. , 2013, , .		Ο
250	Nanometer-scale study of resistance on CdTe solar cell devices. , 2014, , .		0
251	Minority carrier lifetimes in 1.0-eV p-In <inf>0.27</inf> Ga <inf>0.73</inf> As layers grown on GaAs substrates. , 2014, , .		0
252	Cathodoluminescence study of carrier transport across grain boundaries in CdTe. , 2014, , .		0

#	Article	IF	CITATIONS
253	The possibility of optical excitations at the smallest gap of Cu-delafossite nanocrystals. Journal Physics D: Applied Physics, 2014, 47, 405301.	1.3	0
254	Characterization of Photovoltaics: From Cells Properties to Atoms. Microscopy and Microanalysis, 2014, 20, 952-953.	0.2	0
255	Determination of the electrical junction in Cu(In, Ga)Se <inf>2</inf> and Cu <inf>2</inf> ZnSnSe <inf>4</inf> solar cells with 20-nm spatial resolution. , 2016, , .		0
256	Spatial distribution of dopant incorporation in CdTe. , 2016, , .		0
257	Cover Image, Volume 25, Issue 9. Progress in Photovoltaics: Research and Applications, 2017, 25, i.	4.4	0
258	Near-field transport imaging application of photovoltaic materials. , 2017, , .		0
259	Notice of Removal Sodium accumulation at potential-induced degradation shunted areas in polycrystalline silicon modules. , 2017, , .		0
260	Large-Area Junction Damage in Potential-Induced Degradation of c-Si Solar Modules. , 2017, , .		0
261	Large-Area Material and Junction Damage in c-Si Solar Cells by Potential-Induced Degradation. , 2018, , .		0
262	Transmission Electron Microscopy Study on Degradation Mechanism of CdTe Thin-Film Solar Cells. , 2018, , .		0
263	Carrier-Transport Imaging of Cadmium Telluride Intra- and Inter-Grains. , 2018, , .		0
264	Cover Image, Volume 26, Issue 6. Progress in Photovoltaics: Research and Applications, 2018, 26, i-i.	4.4	0
265	Transmission Electron Microscopy Study on Microstructure of Degraded CdTe Mini-Modules. IEEE Journal of Photovoltaics, 2019, 9, 893-897.	1.5	0
266	Extracting optical bandgaps from luminescence images of perovskite solar cells. , 2019, , .		0
267	Microstructure Study on Initial Lithiation/Delithiation Cycle of Crystalline Silicon Wafer—ADDENDUM. Microscopy and Microanalysis, 2020, 26, 183-183.	0.2	0
268	Comparative studies of optoelectronic properties, structures, and surface morphologies for phosphorus-doped poly-Si/SiOx passivating contacts. , 2021, , .		0
269	Trap-Assisted Dopant Compensation Prevents Shunting in poly-Si Passivating Interdigitated Back Contact Silicon Solar Cells. , 2021, , .		0
270	(Photo)electrochemical Characterization of Doped ZnO Electrodes. ECS Meeting Abstracts, 2009, , .	0.0	0

#	Article	IF	CITATIONS
271	Evidence of Buried Junction in CdSeTe Absorbers. , 2020, , .		0
272	Correlative nm-Scale Nonuniformity of Active Charge Carriers and Electrical Potential along both the Plane-View and Depth Directions in Group-V-Doped CdTe Thin Films. , 2020, , .		0